Characterization of iron species in *ex*-framework FeZSM-5 by electrochemical methods

A. Doménech [a], J. Pérez-Ramírez [b,*], A. Ribera [b], F. Kapteijn [b], G. Mul [b], and J.A. Moulijn [b]

[a] *Department of Analytical Chemistry, University of Valencia, Dr. Moliner 50, 46100 Burjassot, Valencia, Spain*
[b] *Industrial Catalysis, DelftChemTech, Delft University of Technology, Julianalaan 136, 2628 BL, Delft, The Netherlands*

Received 10 July 2001; accepted 30 October 2001

Solid state electrochemistry is described as a method to characterize iron species in the different stages of the preparation of *ex*-framework FeZSM-5. The *ex*-framework method comprises the hydrothermal synthesis of isomorphously substituted FeZSM-5, followed by calcination at 823 K and steam treatment (300 mbar H_2O in N_2) at 873 K. Incorporation of FeZSM-5 samples in graphite–polyester composite (GPC) electrodes and identification of the electrochemical response provides information on the structural environment and oxidation state of electroactive iron species in the zeolite. ^{57}Fe Mössbauer spectroscopy and TEM analysis were additionally used to interpret the electrochemical responses. Tetrahedral iron atoms in framework positions were the only species observed in the as-synthesized material. After calcination, also isolated extra-framework iron ions and oligonuclear iron–oxo complexes were identified, as well as a minor amount of FeO_x nano-particles. The steaming procedure leads to extensive formation of the FeO_x nano-particles of 1–2 nm in size, which were also identified by TEM. Both oxidative as well as reductive dissolution processes have been observed for the nano-particles, suggesting the presence of both Fe(II) and Fe(III) oxidation states in the steamed FeZSM-5, which is confirmed by Mössbauer spectroscopy. Tetrahedrally coordinated iron atoms in framework positions, as well as the isolated extra-framework iron ions and oligonuclear iron–oxo complexes in octahedral positions, yield electron-transfer processes that approach that of strongly electrode-attached species with distinctive variations of the electrochemical parameters on the pH and the potential scan rate.

KEY WORDS: FeZSM-5; *ex*-framework method; iron species, electrochemistry; catalysis; characterization

1. Introduction

Fe-based zeolites with MFI structure, including ZSM-5 and silicalite, are receiving increasing attention, due to their catalytic activity in numerous chemical reactions. These processes include isomerization and oxidative dehydrogenation of alkanes [1,2] and selective oxidations of benzene to phenol and methane to methanol, using N_2O as the oxidant [3,4]. FeMFI also plays an important role in environmental catalysis for the removal of gaseous pollutants, namely NO_x (de-NO_x HC-SCR or NH_3-SCR) [5–9], N_2O (direct decomposition or reduction with hydrocarbons or NH_3) [10–13], and NH_3 (selective oxidation to N_2 with O_2) [14].

Various techniques have been described in the literature to characterize Fe-zeolites, including TEM, FT-IR, TPR, ESR, and recently EXAFS [15–23]. Various iron species have been identified in FeZSM-5: isolated ions in framework positions or extra-framework at cationic positions in the zeolite channels, dinuclear and, in general, oligonuclear iron complexes in extra-framework positions, iron oxide nano-particles ($\leq$2 nm), and large iron oxide particles (Fe_2O_3) in a wide distribution (up to 25 nm in size) located at the external surface of the zeolite crystal. There is controversy about the nature of the active Fe sites in the different processes catalyzed by FeZSM-5, due to the heterogeneous nature of the Fe species in the material. In de-NO_x HC-SCR, dinuclear iron species in the channels of the ZSM-5 were suggested to be the active species [3,6,17,18,23], but also oligonuclear complexes of composition Fe_4O_4 (referred to as ultra-stable nano-clusters) have been identified as active redox centers in the same reaction [15].

Some of us recently reported than an *ex*-framework route to prepare FeZSM-5 yields a catalyst with significantly higher activity (on a per Fe basis) than catalysts prepared via other procedures, such as liquid- (aqueous) or solid-ion exchange and sublimation [24,25]. Also the stability in simulated tail-gases from nitric acid plants and fluid-bed combustors is significantly improved. The *ex*-framework method encompasses the hydrothermal synthesis of isomorphously substituted FeZSM-5, followed by calcination and steam treatment (300 mbar H_2O in N_2) at 873 K. Application of different techniques (UV–vis, TEM, and EPR) led to the conclusion that the steam treatment induces the migration of Fe towards extra-framework positions, which was found to be crucial in order to create catalytically active iron species for N_2O decomposition, as well as for phenol productivity in N_2O-mediated oxidation of benzene to phenol [19,25]. Different authors have investigated the extraction of iron from isomorphously substituted Fe-silicalite

* To whom correspondence should be addressed.
E-mail: j.perezramirez@tnw.tudelft.nl

1011-372X/02/0300-0303/0

upon thermal treatment in the range 773–1073 K [26,27]. A detailed physicochemical characterization of the activation of *ex*-framework FeZSM-5 and the nature of the species formed by the steaming procedure has been recently reported [28]. From this study it was concluded that due to the heterogeneous nature of the iron in the catalyst, which is present in different forms and relative amounts, identification of the various iron species requires a combination of suitable spectroscopic techniques.

Electrochemical methods, also referred to as voltammetric techniques, can contribute to the characterization of various iron species in FeZSM-5. Although electrochemical techniques have been traditionally focused on studies in solution, the development of a variety of chemically modified electrodes has prompted systematic studies dealing with the characterization of solid samples. This approach has been labelled as solid state electrochemistry or chemistry of solid microparticles [29–32]. This methodology has been previously applied to the study of the electrochemistry of electroactive species (single metal ions (Ag^+, Cu^{2+})) [33–38] or metal complexes (Mn and Fe-salen, Co-phthalocyanine) [39–44] encapsulated into the channels and cages of different microporous materials (mainly Y zeolite). However, there are no studies concerning the electrochemistry of tetrahedral framework iron, octahedral extra-framework iron species, and/or iron oxide nano-particles in zeolite catalysts.

In this paper we report on the electrochemical characterization of the different iron species existing in FeZSM-5 zeolites using graphite–polyester composite (GPC) electrodes. The shape of the voltammetric responses, in combination with the different electrode preparation methods and the dependency of peak potentials on the pH and potential scan rate, were used to characterize the different Fe electroactive species in isomorphously substituted FeZSM-5, as well as in the corresponding materials obtained after calcination and steam treatment.

2. On the electrochemistry of zeolite-attached species

For non-conducting solid microparticles, the electron-transfer processes occur at the three-phase boundary between the electrolyte solution, the inert electrode, and the solid particle. Charge conservation requires in general an exchange of ions between the solid and the solution phase. Interpretation of electrochemical responses occurring at zeolite-modified electrodes has been a subject of controversy regarding the possible mechanisms for electron transfer to redox electroactive species in zeolites [38,39]. These have been denoted as (i) extrazeolitic; (ii) intrazeolitic; and (iii) surface-mediated electron-transfer processes in the more external zeolite sites, denoted as ''boundary associated'' species [40]. In the extrazeolitic mechanism, the electron transfer process takes place outside of the zeolite after ion exchange of electroactive species with electrolyte cations [34–36]. The intrazeolitic mechanism involves electron transfer processes affecting electroactive species located in the supercages of the outer cavities or subsurface zones of the zeolite [37–43]. Intrazeolitic electron transport and ion transport mechanisms have been also described [38]. We have recently provided evidence that the electrochemical observation corresponds to a ''boundary region'' of the zeolite [45], situated close to the external surface, in agreement with other authors [46]. This implies that the electrochemistry measured not only corresponds to iron oxide particles at the external surface of the crystal, but also to iron species in framework positions or strongly attached to the zeolite (*i.e.*, in the channels).

The analysis of electrochemical response is also complicated by the fact that different electroactive zeolite-associated species can be responsible for the observed electrochemistry. This especially applies to the FeZSM-5 system, where different species, including framework and extra-framework single iron ions, dimeric or oligomeric iron oxo-complexes, iron oxide nano-particles, and large iron oxide particles, co-exist in the sample. Secondly, various topological redox iron isomers at different locations of the zeolite may exist [43,44]. Electroactive extra-framework iron ions can be:

- outside the zeolite, with no bonding or sorptive association;
- bound to the boundary (or external surface) of the zeolite;
- adsorbed into the voids of the zeolite, but able to sample the global pore lattice topology;
- size-included in the interior of a supercage or a channel intersection of the zeolite.

In spite of these difficulties, electrochemical data can be used to discern between different electroactive species. In general, the electrochemical behavior depends on the zeolite and electrode preparation, redox electroactive system, supporting electrolyte, pH, presence of complexing agents, and time-scale of the experiments. The dependence of peak potentials on the pH and potential scan rate, as well as the shape of voltammetric curves and their variation upon the different electrode preparation and the contact time of the modified electrode immersed into the electrolyte solution prior to the electrochemical runs (so-called rest time) can be used as diagnostic criteria.

The observed voltammetric peaks can be ascribed to different theoretical models that provide significant differences in the shape of current-potential curves [45]. Figure 1 shows the theoretical linear scan voltammograms (LSVs) for:

- reversible electron-transfer process involving species in solution;

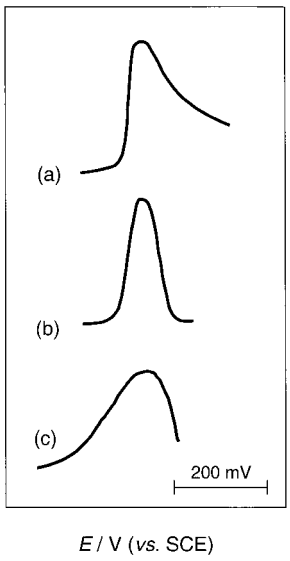

Figure 1. Typical profiles obtained in linear scan voltammograms (LSVs) for (a) reversible electron-transfer process involving species in solution; (b) reversible electron-transfer process between species strongly attached to the electrode surface; and (c) reductive dissolution of a solid.

- reversible electron-transfer process between species attached to the electrode surface;
- reductive dissolution of a solid.

Baker *et al.* [35] explained that electroactive species are electrochemically reduced or oxidized in a thin layer of electrolyte solution existing between the zeolite particles and the electrode. Since electron-transfer steps must be coupled with the release of charge-balancing electrolyte cations, M^+, the overall electrochemical reaction rate may be controlled by the diffusion of such electrolyte cation, and/or by its interchange with zeolite-associated ions, and/or the diffusion of such zeolite-associated species through the channel system. Neglecting electroactive species in the bulk solution, and assuming that diffusion in this layer is fast in comparison to intrazeolite counter diffusion and intracrystalline ion exchange, the system can be treated as a diffusion-controlled process yielding a voltammetric profile similar to that of diffusion-controlled processes in solution. This is characterized by a slow current decrease 100–150 mV past the voltammetric peak [47–49], in the so-called *diffusive region* of the voltammogram (figure 1(a)). The peak potential of this process varies with the potential scan rate.

For an electron-transfer process in which both the oxidized and reduced forms remain strongly attached on the electrode surface, a typical symmetric peak is obtained (figure 1(b)), whose profile is equivalent to that of a classical thin-layer cell with the peak potential independent of the potential scan rate [50].

Among the other possibilities, the reductive or oxidative dissolution of a set of solid microparticles, recently described in detail by Grygar [51], exhibits current–potential curves whose profile depends on the shape and size distribution of the particles. Although the exact voltammetric profile depends on the *polydispersity* of the particle set, typical current–potential curves can be distinguished from those previously described (figure 1(c)). In this case, the peak potential also varies with the potential sweep rate.

3. Experimental

3.1. Catalyst preparation

The isomorphously substituted FeZSM-5 was synthesized hydrothermally using tetrapropylammonium hydroxide as the template [19]. A solution of the silica source (tetraethylorthosilicate, TEOS, Acros, 98%), the template (tetrapropylammonium hydroxide, TPAOH, Fluka, 20% in water), and NaOH was added to a mixture of aluminum(III) nitrate ($Al(NO_3)_3{\cdot}9H_2O$, Merck, 99%) and iron(III) nitrate ($Fe(NO_3)_3{\cdot}9H_2O$, Merck, 98.5%). The molar ratios between components were $H_2O/Si = 45$, $TPAOH/Si = 0.1$, $Na/OH = 0.2$, $Si/Al = 36$, and $Si/Fe = 152$. The solution was transferred to a stainless steel autoclave lined with Teflon and kept in a static air oven at 448 K for 5 days. The crystalline material was filtered and washed with deionized water. The as-synthesized sample (FeZSM-5*as*), in which Fe(III) is isomorphously substituted in the zeolite framework, was calcined in air at 823 K for 10 h and was then converted into the H-form by three consecutive exchanges with an ammonium nitrate solution (0.1 M) overnight and subsequent calcination at 823 K for 5 h (FeZSM-5*c*). Finally, the catalyst was treated in flowing steam at ambient pressure (water partial pressure of 300 mbar and 30 ml min^{-1} of N_2 flow) at 873 K for 5 h, yielding *ex*-FeZSM-5.

3.2. Physicochemical characterization

The chemical composition of the catalysts was determined by ICP-OES (Perkin-Elmer Plasma 40 (Si) and Optima 3000DV (axial)) and AAS (Perkin-Elmer 1100). X-ray diffraction (XRD) analysis was performed with a Bruker AXS diffractometer, using Cu Kα radiation ($\lambda = 0.1541$ nm) and a diffracted beam graphite monochromator. Data were collected in the 2θ range of 5–50° with a step size of 0.1° 2θ and a counting time of 8 s per step scan. Transmission Electron Microscopy (TEM) was carried out on a Philips CM 30 T electron microscope with a LaB_6 filament as the source of electrons operated at 300 kV. In order to enhance the visibility of the small particles, the zeolites were amorphized by the electron beam. This process did not induce sintering of iron oxide particles in the specimen. ^{57}Fe Mössbauer spectra of the different FeZSM-5 samples were obtained on a constant acceleration spectrometer in a triangular mode with a ^{57}Co : Rh source.

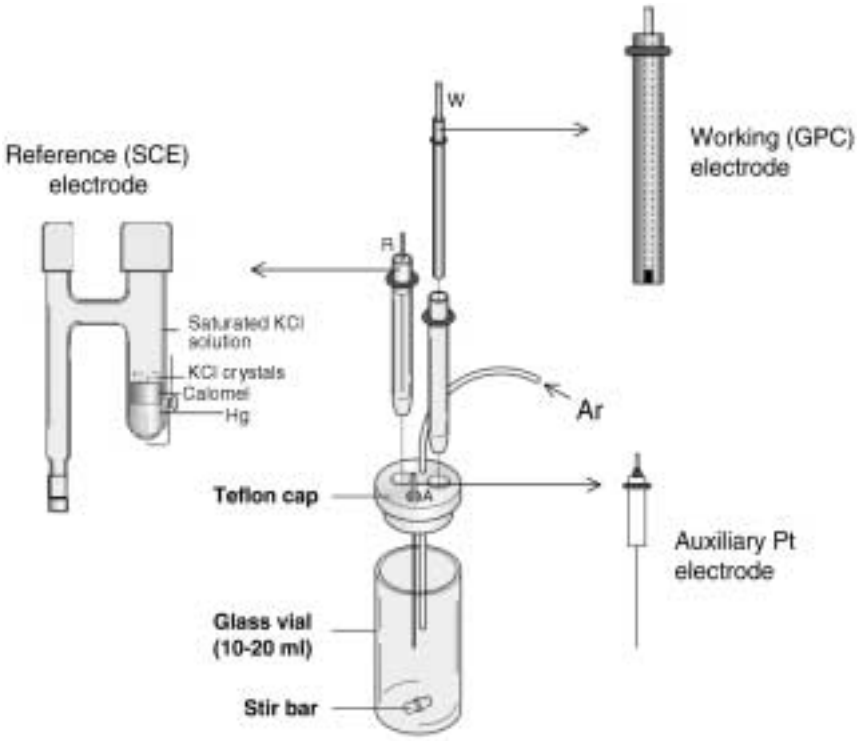

Figure 2. Scheme of the electrochemical cell with the different components.

Spectra were obtained at 300 K in air. The overall spectra were deconvoluted with calculated Mössbauer spectra that consisted of Lorentzian-shape lines. In the case of quadrupole doublets the line widths and the absorption areas of the constituent lines were constrained equal. Positional parameters were not constrained in the fitting procedure. Isomer shift values are reported relative to sodium nitroprusside. The accuracy of positional parameters is $\pm 0.03\,\mathrm{mm\,s^{-1}}$.

3.3. Electrochemical characterization

3.3.1. Preparation of modified electrodes

Graphite–polyester composite electrodes were prepared using graphite powder (Aldrich, 1–2 μm size) and Estratil AL-100 polyester resin dissolved in styrene (33 vol%) acting as reactive monomer. The co-polymerization reaction was catalyzed by cobalt octoate incorporated in the initial prepolymer solution (0.07 vol%) and initiated by adding ethylmethylketone peroxide (2 vol%). The composite electrode was prepared adding 45 wt% graphite to 55 wt% of polyester resin freshly prepared. Zeolite-modified electrodes were prepared by (a) lightly-ground conditioning or (b) abrasive conditioning. Lightly-ground conditioned electrodes were prepared by adding a drop of a suspension of the zeolite (5 mg) in acetone (5 ml) to the surface of the electrode and allowing the solvent to evaporate. Abrasive conditioned electrodes were prepared by placing 1–2 mg of the zeolite sample on a glazed porcelain tile forming a spot of finely distributed material. Abrasive conditioned electrodes were prepared by pressing and vigorously rubbing that spot of sample over the lower end of the electrode. Preparation of electrodes by abrasive conditioning involves further crushing of zeolite particles, leading to a relative enhancement of the number of electrochemically accessible iron species and thus increasing the intensity of voltammetric peaks.

3.3.2. Instrumentation and procedures

The electrochemical experiments were carried out in a standard three-electrode cell (figure 2) consisting of a working electrode (graphite–polyester composite electrode modified with the FeZSM-5 samples, a platinum auxiliary electrode, and a saturated calomel reference electrode (SCE). Experiments were performed at 298 K after the immersion of the electrodes in the electrolyte (aqueous) solution under Ar atmosphere and constant stirring, with a rest time of 0–10 min. Aqueous solutions of HCl (Probus) and NaCl (Probus) with a total concentration of 0.1–1.0 M were used as supporting electrolyte, with pH values ranging from 0.0 to 3.0. Hematite (Fe_2O_3, Alfa, >99%), Goethite (FeOOH, Fluka, 99%), and $FeCl_3{\cdot}6H_2O$ (Panreac, >98.5%) were used as reference materials. Linear scan voltammograms (LSVs) and differential pulse voltammograms (DPVs) were performed at potential scan rates (ν) ranging from 1 to $200\,\mathrm{mV\,s^{-1}}$ (normally $\nu = 20\,\mathrm{mV\,s^{-1}}$) using a Metrohm E506 Polarecord. The pulse amplitude (ΔU) in the DPVs was 80 mV.

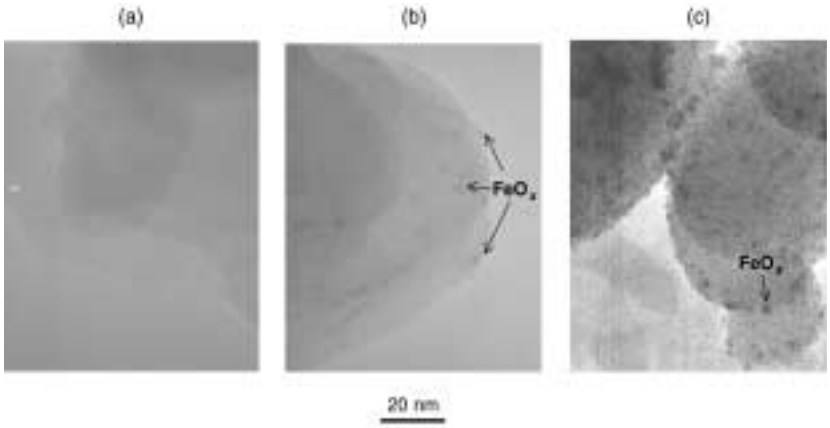

Figure 3. TEM micrographs of (a) FeZSM-5*as*; (b) FeZSM-5*c*; and (c) *ex*-FeZSM-5.

4. Results and discussion

4.1. Physicochemical characterization

The elemental analysis of the as-synthesized (FeZSM-5*as*), calcined (FeZSM-5*c*), and steamed (*ex*-FeZSM-5) samples is given in table 1. Comparison of the composition of the synthesis gel and the crystalline samples during preparation of the *ex*-framework FeZSM-5 indicates that all the iron and aluminum are present in the solid, while a small part of the silicon is not incorporated. Only minor differences between the as-synthesized sample and the post-treated samples (calcined and steamed) can be observed. The concentration of Na in the calcined and steamed samples is below detection limits.

TEM and ^{57}Fe Mössbauer spectroscopy were used to investigate the extraction of the Fe ions from the zeolite lattice upon calcination and steam treatment. The TEM micrograph of FeZSM-5*as* does not show any iron-related phase (figure 3(a)), suggesting that all the Fe(III) is present in a highly dispersed state at isolated positions in the zeolite framework of the as-synthesized material. Calcination of FeZSM-5*as* to yield FeZSM-5*c* extracts some isomorphously substituted Fe to non-framework positions, as concluded from the presence of small iron oxide particles in the TEM micrograph of FeZSM-5*c* (figure 3b). Steam treatment massively dislodges iron to non-framework positions, inducing the formation of homogeneously dispersed iron oxide nano-particles of 1–2 nm (figure 3(c)). It has been previously shown [19] that the long-range crystalline order of the zeolite is not affected by calcination and steam treatment. No evidence of any other phases besides ZSM-5 was found in the XRD of these samples. The absence of a hematite phase can be related to (i) the small amount of Fe_2O_3 present (Fe loading is 0.67 wt% in the steamed catalyst), (ii) line broadening due to very small crystallite particles, and (iii) the dislodged iron as Fe_2O_3 remains amorphous.

^{57}Fe Mössbauer spectra of as-synthesized, calcined, and steamed FeZSM-5 samples recorded at 300 K in air are shown in figure 4. The spectrum of FeZSM-5*as* (figure 4(a)) shows a broad singlet with an average isomer shift, IS = 0.52 mm s^{-1}, which has been assigned to tetrahedrally coordinated Fe(III) ions [52]. Such a broad singlet is typical for paramagnetic iron ions with slow electron spin relaxation, implying large Fe–Fe distances, and thus a homogeneous distribution of Fe(III) ions in the ZSM-5 framework. After calcination of the sample a considerable narrowing of the Mössbauer signal is observed together with the onset of a

Table 1.
Chemical composition of the crystalline samples used in this study

Sample	Si/Al	Si/Fe	Na (wt%)	Fe (wt%)
FeZSM-5*as*[a]	31.1	126.2	0.44	0.59
FeZSM-5*c*	31.6	124.9	0.00	0.64
ex-FeZSM-5	31.3	121.7	0.00	0.67

[a] Metal molar ratio in the synthesis gel: Si/Al = 36 and Si/Fe = 152.

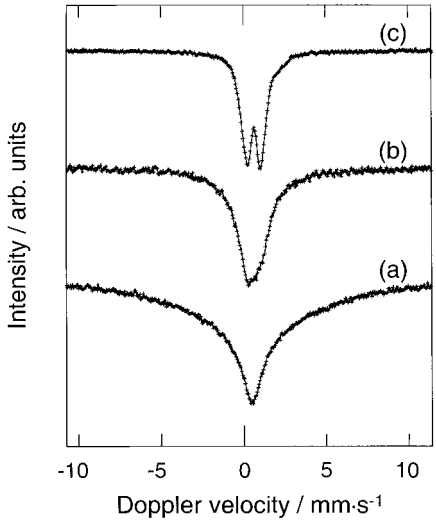

Figure 4. ^{57}Fe Mössbauer spectra of (a) FeZSM-5*as*; (b) FeZSM-5*c*; and (c) *ex*-FeZSM-5. Measurements were carried out in air at 300 K.

paramagnetic doublet (figure 4(b)). This is the result of shortened electron spin relaxation times, indicating a shortening of the Fe–Fe distances. This suggests that calcination leads to removal of Fe(III) ions from the ZSM-5 framework. The extra-framework species may reside in cationic positions, form small iron–oxo complexes, and to a minor extent, cluster in small nanoparticles, as shown in the TEM micrograph of FeZSM-5*c* (figure 3(b)).

Steam treatment leading to *ex*-FeZSM-5 subsequently gives rise to a well-resolved paramagnetic doublet with an $IS = 0.59\,mm\,s^{-1}$ and quadrupole splitting, $QS = 0.90\,mm\,s^{-1}$ (figure 4(c)). The observation of a well-resolved doublet indicates a further increase in electron spin relaxation rates and is interpreted by a continued clustering of Fe(III) ions and small iron–oxo complexes into larger particles. In addition, a small shoulder on the high-energy line of this doublet is fitted with a second doublet with $IS = 1.30\,mm\,s^{-1}$ and $QS = 1.59\,mm\,s^{-1}$. The IS of this doublet suggests that a small part of the iron is present as Fe(II) in the steamed *ex*-FeZSM-5 (10% according to the spectral fitting). The presence of Fe(II) in the steamed catalysts will be further discussed in the next section.

4.2. Electrochemical response

4.2.1. General voltammetric patterns

Figure 5 shows a series of cathodic differential pulse voltammograms (DPVs) for graphite-polyester composite (GPC) electrodes modified by (a) FeZSM-5*as*; (b) FeZSM-5*c*; (c) *ex*-FeZSM-5; (d) hematite; and (e) goethite immersed in 1.0 M HCl aqueous solution. The voltammetric responses presented in this manuscript were reproducible (repeated at least three times). For FeZSM-5*as*, only the peaks C_4 (+0.05 V *versus* SCE) and C_5 (−0.15 V *versus* SCE) are well defined. *Ex*-FeZSM-5 exhibits a relatively complicated electrochemical pattern. In this sample, the peaks C_4 and C_5 are not visible and new reduction peaks at +0.65 (C_1), +0.35 (C_2), +0.28 (C_3), −0.55 (C_6) and −0.75 (C_7) V *versus* SCE appear. FeZSM-5*c* shows a voltammogram in between that of FeZSM-5*as* and *ex*-FeZSM-5. In the latter sample, the signals of both the as-synthesized and steamed samples are present, but with a relatively low intensity. This indicates a progressive transition of the electroactive iron species from the as-synthesized to the calcined zeolites, and further to the final steamed catalyst.

The results in figure 5 already indicate that the electrochemistry of iron species in FeZSM-5 zeolites shows significant differences compared to that of iron oxides and hydrous oxides. GPC electrodes modified with hematite and goethite show prominent cathodic peaks in the range from −0.25 to −0.80 V *versus* SCE (C_6 and C_7). By comparison of the different patterns, it appears that only the electrode process C_6 recorded in *ex*-FeZSM-5 can correspond to a reductive dissolution process involving iron oxide nano-particles of 1–2 nm, which were identified by TEM analysis (figure 3(c)).

A more detailed view of the electrochemical response of FeZSM-5-modified electrodes is presented in figure 6, in which cathodic (C) and anodic (A) linear scan voltammograms (LSVs) for GPC electrodes modified by *ex*-FeZSM-5 (a and b) and FeZSM-5*as* (c and d) immersed in 0.10 M HCl aqueous solutions are shown.

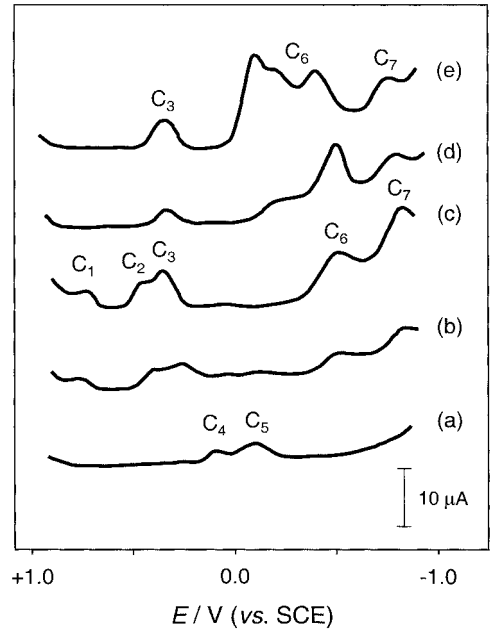

Figure 5. Cathodic DPVs for (a) FeZSM-5*as*; (b) FeZSM-5*c*; (c) *ex*-FeZSM-5; (d) hematite; and (e) goethite, attached to GPC electrodes immersed in 1 M HCl aqueous solution; $\nu = 20\,mV\,s^{-1}$, $\Delta U = 80\,mV$.

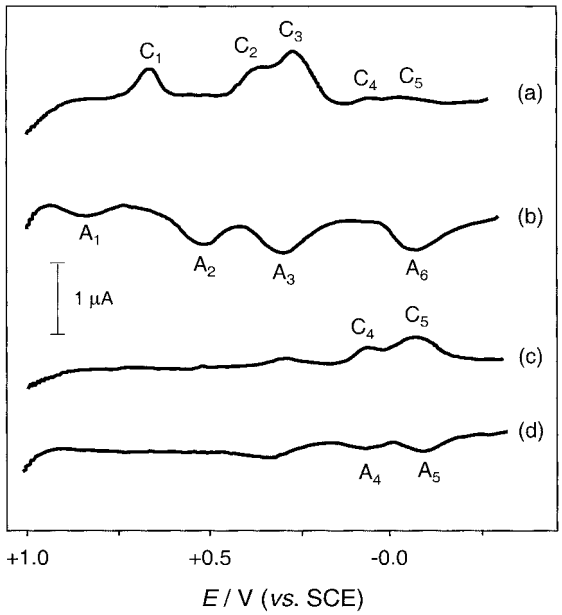

Figure 6. Cathodic (a, c) and anodic (b, d) LSVs for GPC electrodes modified by (a, b) *ex*-FeZSM-5 and (c, d) FeZSM-5*as*, immersed in 0.10 M HCl aqueous solution. Abrasive-conditioned electrodes. Contact time 5 min; $\nu = 20\,mV\,s^{-1}$.

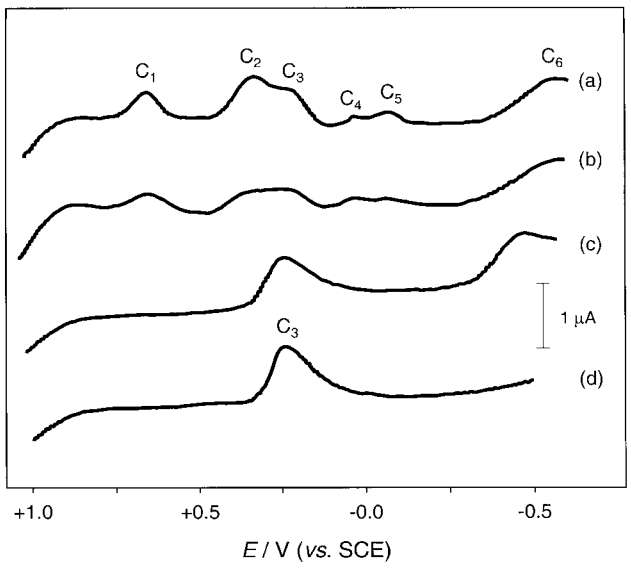

Figure 7. Cathodic LSVs for *ex*-FeZSM-5 modified GPC electrodes in 0.10 M HCl aqueous solution upon (a) abrasive conditioning, contact time 5 min; (b) abrasive conditioning, contact time 1 min; and (c) lightly-ground conditioning, contact time 5 min. Curve (d) corresponds to the response of a 0.50 mM $FeCl_3 \cdot 6H_2O$ and 0.10 M HCl aqueous solution at a bare GPC electrode; $\nu = 20\,mV\,s^{-1}$.

As previously shown, peaks C_1-C_3 are very well defined in *ex*-FeZSM-5, while peaks C_4 and C_5 virtually disappear after the steam treatment. In anodic scans initiated at −0.50 V *versus* SCE over *ex*-FeZSM-5, anodic peaks at −0.18 (A_6), +0.36 (A_3), +0.42 (A_2) and +0.73 (A_1) V *versus* SCE appear. Peaks A_6 and A_3 obscure the anodic counterparts of peaks C_4 and C_5, *i.e.*, A_4 and A_5, respectively. This response is in contrast with that obtained for FeZSM-5*as*, where only the C_4/A_4 and C_5/A_5 couples clearly appear. Since all iron ions in FeZSM-5*as* are tetrahedrally coordinated in the zeolite framework (isomorphous substitution), as can be concluded from the ^{57}Fe Mössbauer spectrum and TEM micrograph of the as-synthesized sample, such electrochemical couples must be attributed to redox processes involving framework iron species.

As shown in figure 7, the peak C_3 in *ex*-FeZSM-5 (which is also present in goethite and hematite, figure 5) is close to that observed in solutions of $FeCl_3 \cdot 6H_2O$ in acidic media (0.1 M HCl) at a bare GPC electrode (compare pattern a and d). Accordingly, this peak in the solid samples can be attributed to redox processes involving iron ions present in solution resulting from reductive and oxidative dissolution processes and the leaching of iron ions in the more external surface of the zeolite, probably in exchangeable positions. On the other hand, peaks C_1 and C_2 in *ex*-FeZSM-5 likely correspond to relatively small extra-framework species strongly attached to the zeolite, which are formed during the activation (calcination and steaming) of the isomorphously substituted FeZSM-5. These assignments are discussed below, and the electrochemical processes involved are summarized in table 2.

4.2.2. Electrochemistry of iron oxide nano-particles

The electrode process C_6, which is characteristic of *ex*-FeZSM-5, exhibits electrochemical parameters close to those described for the reductive dissolution of iron oxides and hydroxy-oxides (figure 1(c)) [51]. In particular, peak potentials of C_6 show a linear dependency with the pH of the supporting electrolyte and the logarithm of the potential scan rate, $\log \nu$ (at a constant pH), as depicted in figures 8(a) and 9(a) (empty circles), respectively. The same behavior was observed in hematite and goethite (figures 8(b)–(d) and 9(b)–(d), solid diamonds). Accordingly, the reduction of iron oxide nano-particles generated during preparation of *ex*-FeZSM-5 can be represented as:

$$Fe^{III}O_x + 2xH^+ + (2x + n - 3)e^- \rightarrow (1-n)Fe^{3+}(aq.) + nFe^{2+}(aq.) + xH_2O \qquad (1)$$

where n represents the fraction of Fe(III) effectively reduced to Fe(II). Under sufficiently acidic conditions, $n = 1$. The peak C_7 present in *ex*-FeZSM-5, as well as in hematite and goethite, accounts for the metal

Table 2
Summary of the electrochemical processes involving iron species in the FeZSM-5 system. Peak potentials (E_p) in mV *versus* SCE from LSVs in 0.10 M HCl electrolyte; $\nu = 20\,mV\,s^{-1}$

Peak	E_p (mV)	Species involved	Assignment [a]	Electrochemical process
C_4/A_4 C_5/A_5	+50 −150	Framework Fe-ions	YE	$Z[O_3Fe^{III}(OH)](b) + M^+(aq.) + e^- \rightleftharpoons Z[O_3Fe^{II}(OH)](b) + M^+(b)$
C_1/A_1	+650	Oligonuclear Fe–oxo complexes	YE	$Z\text{-}Fe^{III}_xO_y(b) + xH^+(aq.) + xe^- \rightleftharpoons Z\text{-}Fe^{II}_xO_{y-x}(OH)_x(b)$
C_2/A_2	+300	Isolated Fe-ions	YE	$Fe^{I}I\text{-}Z(b) + M^+(aq.) + e^- \rightleftharpoons Fe^{II}\text{-}Z + M^+\text{-}Z(b)$
C_6	−550	FeO_x nano-particles	RD	$Fe^{III}O_x + 2xH^+(aq.) + (2x-2)e^- \rightarrow Fe^{2+}(aq.) + xH_2O$
C_7	−750		MD	$Fe^{2+}(aq.) + 2e^- \rightarrow Fe^o$
A_6	−180		OD	$Fe^{II}O_y + 2yH^+(aq.) \rightarrow Fe^{3+}(aq.) + yH_2O + (3-2y)e^-$
C_3/A_3	+280/+360		D	$FeCl_x^{(3-x)+} + e^- \rightleftharpoons FeCl_y^{(2-y)+} + (x-y)Cl^-$

Z: zeolite; (b): sites at the boundary of the zeolite; M^+: charge compensating cation

[a] YE: electron-transfer process on iron species attached to the zeolite boundary; RD: reductive dissolution; MD: metal deposition; OD: oxidative dissolution; D: electron-transfer process involving species in solution.

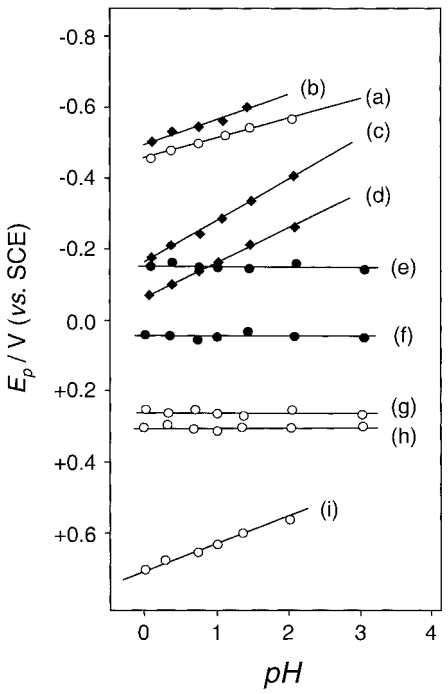

Figure 8. Peak potential (E_p) *versus* pH for zeolite-modified GPC electrodes immersed in HCl + NaCl aqueous solutions (total concentration 1.0 M); (a) *ex*-FeZSM-5, peak C_6; (b) hematite, peak C_6; (c) and (d) goethite, overlapped peaks C_6; (e) FeZSM-5*as*, peak C_5; (f) FeZSM-5*as*, peak C_4; (g) *ex*-FeZSM-5, peak C_3; (h) *ex*-FeZSM-5, peak C_2; (i) *ex*-FeZSM-5, peak C_1. Peak potentials from LSVs at $\nu = 20\,\mathrm{mV\,s^{-1}}$.

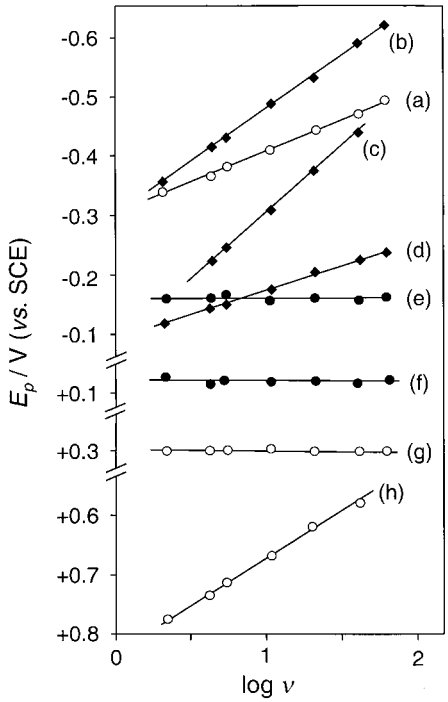

Figure 9. Peak potential (E_p) *versus* the logarithm of the potential scan rate ($\log \nu$) for zeolite-modified GPC electrodes immersed in 0.10 M HCl aqueous solutions; (a) *ex*-FeZSM-5, peak C_6; (b) hematite, peak C_6; (c) and (d) goethite, overlapped peaks C_6; (e) FeZSM-5*as*, peak C_5; (f) FeZSM-5*as*, peak C_4; (g) *ex*-FeZSM-5, peak C_2; and (h) *ex*-FeZSM-5, peak C_1. Peak potentials from LSVs at $\nu = 20\,\mathrm{mV\,s^{-1}}$.

deposition of the dissolved ions. For $n = 1$, that is:

$$Fe^{2+} + 2e^- \rightarrow Fe^o \qquad (2)$$

The anodic process A_6 in *ex*-FeZSM-5 (figure 6(b)) has been attributed to the oxidative dissolution of iron(II) nano-particles [45]:

$$Fe^{II}O_y + 2yH^+ \rightarrow (1-n)Fe^{2+}(aq.) + nFe^{3+}(aq.) + yH_2O + (n+2-2y)e^- \qquad (3)$$

The oxidative dissolution involves the presence of iron(II) nano-particles, suggesting the presence of both Fe(III) and Fe(II) oxidation states in *ex*-FeZSM-5. This result is in line with the Fe(II) contribution identified in the Mössbauer spectrum of the fresh *ex*-FeZSM-5 sample at 300 K in air (see figure 4(c)). The reduction of a fraction of Fe(III) to Fe(II) should be due to the steam treatment, where H_2O in inert N_2 was passed through the catalyst at relatively high temperature (873 K). The formation of Fe(II) in FeZSM-5 zeolites has been explained by autoreduction, *i.e.*, the facile interconversion between Fe(III) and Fe(II) in the zeolite upon thermal treatment (>523 K) in inert or vacuum [15,53–55]. Lobree *et al.* [55] recently explained that the reduction process involves release of molecular oxygen and dehydration of initially present $[Fe(OH)_2]^+Z^-$, leading to the formation of $[Fe(OH)]^+Z^-$. It is likely that the presence of H_2O during the steam treatment lowers the extent of Fe(III) reduction, since heat treatment of the steamed sample in dry helium at 623 K for 2 h leads to reduction of 50% of the present Fe(III) to Fe(II) [28]. The possibility of the reduction process being due to the contact of the zeolite with the electrolyte can be ruled out, as concluded from analyses of the zeolite sample obtained after contact with such electrolyte during times corresponding to electrochemical measurements. This could also be concluded from the fact that in the calcined FeZSM-5*c* sample peak A_6 was not identified, indicating that the formation of Fe(II) is purely due to the steam treatment.

4.2.3. *Electrochemistry of framework Fe species*

The C_4/A_4 and C_5/A_5 couples, which are mainly visible in the isomorphously substituted FeZSM-5*as* sample, can be assigned to electron-transfer processes involving framework iron atoms. The peak potentials are essentially pH-independent (figures 8(e), (f), solid circles), suggesting that protonation/deprotonation processes are not included in the rate-determining electrochemical reaction. In parallel, peak potentials are independent of the potential scan rate (figures 9(e), (f), solid circles), as expected for the case of electroactive species strongly attached to the electrode surface or confined to a thin layer on the electrode. The voltammetric profiles are close to that shown in figure 1(b), suggesting that the electrochemical process involves iron species strongly bound to the zeolite. The existence of two couples can

be attributed to two different framework redox isomers having quite similar coordination environments. A similar situation has been recently reported by Venkatathri *et al*. [56] for vanadium-containing zeolites. The electroactive iron species can be described here in terms of $O_3Fe(OH)$ centers, similar to the $O_3Ti(OH)$ redox isomers identified in TS-1 (titanium silicalite-1) [57–59]. The redox process of these iron centers, which should be located in a boundary region of the zeolite framework, can be represented as:

$$Z[O_3Fe^{III}(OH)](b) + M^+(aq.) + e^- \rightleftharpoons Z[O_3Fe^{II}(OH)](b) + M^+(b) \quad (4)$$

where Z is the ZSM-5 zeolite and (b) denotes the sites at the boundary of the zeolite and M^+ is a charge-balancing electrolyte cation.

4.2.4. Electrochemistry of extra-framework Fe species

As previously discussed [45], the couple C_2/A_2 is attributable to a redox process involving extra-framework iron ions in the zeolite boundary:

$$Fe^{III}\text{-}Z(b) + M^+(aq.) + e^- \rightleftharpoons Fe^{II}\text{-}Z(b) + M^+\text{-}Z(b) \quad (5)$$

whereas the couple C_3/A_3 should correspond to an electron-transfer step involving iron ions in solution as suggested by the presence of this couple in LSVs recorded over a bare GPC electrode immersed into a diluted solution of $FeCl_3 \cdot 6H_2O$ in 0.10 M HCl (figure 7(d)). The presence of this couple in voltammograms of zeolite-modified electrodes results from the leaching of iron ions located in the more external sites of the zeolite, in agreement with literature data for zeolite-encapsulated complexes [43,60]. This is experimentally supported by the variation observed in the electrochemical response of *ex*-FeZSM-5 with the mechanical work imparted to the sample and the contact time of the modified electrode immersed into the supporting electrolyte (figure 7). Accordingly, for abrasive-conditioned *ex*-FeZSM-5 (figure 7(a), (b)) all peaks C_1–C_6 are well defined, whereas for lightly-ground conditioned *ex*-FeZSM-5 (figure 7(c)) only the peaks C_3 and C_6 can be clearly distinguished. On prolonging the contact time between the electrode and the electrolyte, the intensity of the peaks is enhanced, as can be seen on comparing figure 7(a) and (b). In agreement with the foregoing considerations, peaks C_3 and A_3 exhibit a typical "diffusive" behavior (figure 1(a)), and can be attributed to a redox process involving iron–chloride complexes in solution resulting from leaching and reductive/oxidative dissolution processes. The peak potential of the electrode process is independent of the pH (figure 8(g), empty circle), and can be represented as:

$$Fe^{III}Cl_x^{(3-x)+} + e^- \rightleftharpoons Fe^{II}Cl_y^{(2-y)+} + (x-y)Cl^- . \quad (6)$$

The peak potential of the couple C_1/A_1 follows a linear dependency with the pH and the potential scan rate (figures 8(i) and 9(h) (empty circles), respectively). In addition, the voltammetric curves exhibit a symmetric shape, which is characteristic of species strongly attached to the electrode surface. We have tentatively assigned the response to small iron oxo-complexes in the zeolite channels that remain attached to the zeolite boundary. These species undergo a rate-determining protonation process couple with the electron-transfer step, as suggested by the slope of the E_p *versus* pH dependency (65 mV).

$$Z\text{-}Fe_x^{III}O_y(b) + xH^+(aq.) + xe^- Z\text{-}Fe_x^{II}O_{y-x}(OH)_x(b). \quad (7)$$

The couple C_2/A_2 also approaches the response of electrode-attached species (figure 1(b)). In this case, peak potentials vary linearly with the potential scan rate but are independent of the pH (figures 8(h) and 9(g) (empty circles), respectively). This couple is attributed to a redox process involving isolated iron ions in cationic positions of the zeolite. This behavior, which has been previously reported for Mn (salen) complexes encapsulated in the channels of zeolite Y (66), can be represented by:

$$Fe^{III}\text{-}Z(b) + M^+(aq.) + e^- Fe^{II}\text{-}Z + M^+\text{-}Z(b). \quad (8)$$

5. Conclusions

Electrochemical response techniques in combination with TEM and ^{57}Fe Mössbauer spectroscopy have been used to characterize various iron species in the different stages of preparation of *ex*-framework FeZSM-5. Electrochemical characterization of the different stages of preparation of *ex*-framework FeZSM-5 provides unique information with respect to iron species in the material. Different species can be identified at the same time, including iron oxide nanoaggregates, tetrahedrally coordinated framework iron atoms, octahedrally coordinated extra-framework iron ions, and iron–oxo complexes located at the boundary region of the zeolite. Characteristic iron-centered electrode processes can be described for different electroactive species on the basis of the shape of voltammetric curves and the variation of electrochemical parameters on the pH and potential scan rate. Accordingly, distinctive electrochemical responses can be obtained. Fe(III) nano-particles display reductive dissolution processes, while Fe(II) nano-particles lead to oxidative dissolution processes. Tetrahedral iron atoms in framework positions, and iron species in the zeolite channels (in the form of isolated exchangeable atoms or as oligomeric iron oxo-complexes attached to the zeolite boundary) yield electron-transfer processes that approach that of strongly electrode-attached species with distinctive

variations of the electrochemical parameters on the pH and potential scan rate.

Acknowledgments

This research was financially supported by the Council for Chemical Science of the Netherlands Organization for Scientific Research (CW-NWO). Dr. P.J. Kooyman and Dr. A.R. Overweg are gratefully acknowledged for performing the TEM and Mössbauer spectroscopic studies, respectively.

References

[1] P.B. Venuto, Microporous Mater. 2 (1994) 297.
[2] Md. Uddin, T. Komatsu and T. Kashima, J. Catal. 150 (1994) 439.
[3] G.I. Panov, A.K. Uriarte, M.A. Rodkin and V.I. Sobolev, Catal. Today 41 (1998) 365.
[4] K.A. Dubkov, V.I. Sobolev and G.I. Panov, Kinet. Catal. 39 (1998) 72.
[5] X. Feng and W.K. Hall, Catal. Lett. 41 (1996) 45.
[6] H.-Y. Chen and W.M.H. Sachtler, Catal. Today 42 (1998) 73.
[7] M. Kögel, R. Mönnig, W. Schwieger, A. Tissler and T. Turek, J. Catal. 182 (1999) 470.
[8] A.-Z. Ma and W. Grünert, Chem. Commun. (1999) 71.
[9] R.Q. Long and R.T. Yang, J. Catal. 188 (1999) 332.
[10] F. Kapteijn, G. Marbán, J. Rodríguez-Mirasol and J.A. Moulijn, J. Catal. 167 (1997) 256.
[11] C. Pophal, T. Yogo, K. Yamada and K. Segawa, Appl. Catal. B 16 (1998) 177.
[12] G. Centi and F. Vazanna, Catal. Today 53 (1999) 683.
[13] M. Mauvezin, G. Delahay, F. Kißlich, B. Coq and S. Kieger, Catal. Lett. 62 (1999) 41.
[14] R.Q. Long and R.T. Yang, Chem. Commun. (2000) 1651.
[15] R. Joyner and M. Stockenhuber, J. Phys. Chem. B 103 (1999) 5963.
[16] M. Rauscher, K. Kesore, R. Mönnig, W. Schwieger, A. Tißler and T. Turek, Appl. Catal. A 184 (1999) 249.
[17] P. Marturano, L. Drozdová, A. Kogelbauer and R. Prins, J. Catal. 192 (2000) 236.
[18] A.A. Battiston, J.H. Bitter and D.C. Koningsberger, Catal. Lett. 66 (2000) 75.
[19] A. Ribera, I.W.C.E. Arends, S. de Vries, J. Pérez-Ramírez and R.A. Sheldon, J. Catal. 195 (2000) 287.
[20] R.Q. Long and R.T. Yang, J. Catal. 194 (2000) 80.
[21] E.M. El-Malki, R.A. van Santen and W.M.H. Sachtler, J. Phys. Chem. B 103 (1999) 4611.
[22] H-Y. Chen, X. Wang and W.M.H. Satchler, Phys. Chem. Chem. Phys. 2 (2000) 3083.
[23] E.M. El-Malki, R.A. van Santen and W.M.H. Sachtler, J. Catal. 196 (2000) 212.
[24] J. Pérez-Ramírez, F. Kapteijn, G. Mul and J.A. Moulijn, Chem. Commun. 694 (2001).
[25] J. Pérez-Ramírez, F. Kapteijn, G. Mul and J.A. Moulijn, Appl. Catal. B (2001) in press.
[26] S. Bordiga, R. Buzzoni, F. Geobaldo, C. Lamberti, E. Giamello, A. Zecchina, G. Leofanti, G. Petrini and G. Tozzola, J. Catal. 158 (1996) 486.
[27] P. Fejes, J.B. Nagy, J. Halász and A. Oszkó, Appl. Catal. A 175 (1998) 89.
[28] J. Pérez-Ramírez, G. Mul, F. Kapteijn, J.A. Moulijn, A.R. Overweg, A. Doménech, A. Ribera and I.W.C.E. Arends (2001) submitted to J. Catal.
[29] F. Scholz and B. Lange, Trends. Anal. Chem. 11 (1992) 359.
[30] F. Scholz and B. Meyer, Chem. Soc. Rev. 23 (1994) 341.
[31] P.G. Bruce, *Solid State Electrochemistry* (Cambridge University Press, Cambridge, 1995).
[32] F. Scholz and B. Meyer, in: *Electroanalytical Chemistry, A Series of Advances*, eds. A.J. Bard and I. Rubinstein, Vol. 20 (Marcel Dekker, New York, 1998) p. 1.
[33] P.K. Dutta and M. Ledney, Progr. Inorg. Chem. 44 (1997) 209.
[34] M.D. Baker, C. Senaratne and J. Zhang, J. Chem. Soc. Faraday Trans. 88 (1992) 3187.
[35] M.D. Baker, C. Senaratne and J. Zhang, J. Phys. Chem. 98 (1994) 1668.
[36] M.D. Baker, J. Phys. Chem. 99 (1995) 12367.
[37] J.-W. Li and G. Calzaferri, J. Electroanal. Chem. 377 (1994) 163.
[38] J.-W. Li, K. Pfanner and G. Calzaferri, J. Phys. Chem. 99 (1995) 2119.
[39] F. Bedioui, E. De Boysson, J. Devynck and K.J. Balkus, J. Electroanal. Chem. 315 (1991) 313.
[40] F. Bedioui, E. De Boysson, J. Devynck and K.J. Balkus, J. Chem. Soc. Faraday Trans. 87 (1991) 3831.
[41] L. Gaillon, N. Sajot, F. Bedioui, J. Devynck and K.J. Balkus, J. Electroanal. Chem. 345 (1993) 157.
[42] F. Bedioui, L. Roué, E. Briot, J. Devynck, S.L. Bell and K.J. Balkus, J. Electroanal. Chem. 373 (1994) 19.
[43] G. Calzaferri, M. Lanz and J.-W. Li, Chem. Commun. (1995) 1313.
[44] N.J. Turro and M. Garcia-Garibay, in: *Photochemistry in Organized Media*, ed. V. Ramamurthy (VCH, New York, 1991) p. 1.
[45] A. Doménech, J. Pérez-Ramírez, A. Ribera, G. Mul, F. Kapteijn and I.W.C.E. Arends, J. Electroanal. Chem. (2001) in press.
[46] C.A. Bessel and D.R. Rolison, J. Phys. Chem. B 101 (1997) 1148.
[47] R.S. Nicholson and I. Shain, Anal. Chem. 36 (1964) 706.
[48] G. Ginzburg, Anal. Chem. 50 (1978) 375.
[49] B.R. Eggins and N.H. Smith, Anal. Chem. 51 (1979) 2282.
[50] A.J. Bard and L.R. Faulkner, *Electrochemical Methods* (John Wiley & Sons, New York, 1980).
[51] T. Grygar, J. Electroanal. Chem. 405 (1996) 117.
[52] A. Meagher, V. Nair and R. Szostak, Zeolites 8 (1988) 3.
[53] R.L. Garten, W.N. Delgass and M. Boudart, J. Catal. 19 (1970) 90.
[54] P. Fejes, J.B. Nagy, K. Lázár and J. Halász, Appl. Catal. A. 190 (2000) 117.
[55] L.J. Lobree, I.-C. Hwang, J.A. Reimer, A.T. Bell, J. Catal. 186 (2001) 242.
[56] N. Venkatathri, M.P. Vinod, K. Vijayamohanan and S. Sivasanker, J. Chem. Soc. Faraday Trans. 92 (1996) 473.
[57] S. de Castro Martins, A. Tuel and Y. Ben Taârit, Stud. Surf. Sci. Catal. 84 (1994) 501.
[58] F. Geobaldo, S. Bordiga, A. Zecchina, E. Gianello, G. Leofanti and G. Petrini, Catal. Lett. 16 (1992) 109.
[59] A.V. Arbuznikov and G.M. Zhidomirov, Catal. Lett. 40 (1996) 17.
[60] C.P. Horwitz, S.E. Creager and R.W. Murray, Inorg. Chem. 1006 (1990) 29.
[61] A. Doménech, P. Formentín, H. García and M.J. Sabater, 2001 submitted to J. Phys. Chem. B.